DOI: 10.15480/882.9358

Eighth International Symposium on Marine Propulsors
smp'24, Berlin, Germany, March 2024

Numerical Investigation of Unsteady Pitching Foil Cavitation

Zhaoyuan Wang, Sungtek Park, Frederick Stern

IIHR—Hydroscience & Engineering, The University of Iowa, Iowa City, Iowa, USA

ABSTRACT

In the present study, numerical simulations of the unsteady cavitation flows around a pitching foil are performed with a focus on the effects of the pitching motion on the cavity behavior and forces. Sinusoidal pitching motions are imposed to the foil with the reduced frequencies and amplitude in the same range of most practical propeller applications. It has been found that the maximum cavity length decreases with the reduced frequency first and then increases, which is in good agreement with the experimental observations. The simulation results show that the cavity is very unstable at low oscillating frequencies and tends to be stable at high frequencies. The force exhibits the same oscillating frequency and phase as the angle of attack. The amplitude of the lift increases with the frequency, and the mean value of the lift decreases with the frequency first and then increases. The numerical issues and challenges of the simulations of the forced unsteady cavitation flows are addressed. Future work will be focused on scale resolved turbulence and more advanced cavitation models.

Keywords

Unsteady cavitation, pitching foil, oscillation, CFD.

1 INTRODUCTION

Cavitation and ventilation can be observed on surface piercing propellers, waterjets, and hydrofoils used for high-speed small craft. Cavitation occurs when the local pressure of water drops below the vapor pressure, while ventilation is due to the air entrainment. These phenomena involve interactions between three phases (air, water, and water vapor) and occur in the turbulent boundary layer on complex geometries (Stern et al 2022; Park 2022), as depicted in Figure 1. Numerical simulations of such flow problems with both cavitation and ventilation are challenging and difficult. In the recent studies by Wang and Stern (2022) and Wang et al (2022), a unique numerical method has been developed for studying these three-phase flow interactions. The geometric VOF method is combined with mixture-based cavitation models. A cavitation implementation algorithm is developed using a pressure-based method for incompressible flows. An algorithm for the three-phase (air, water, and vapor) interactions is also developed. Numerical tests, including both 2D and 3D steady and unsteady cavitation flows (with fixed bodies), have been conducted. The method has also been applied to investigate super-cavitating surface-piercing hydrofoils (Brizzolara et al 2022).

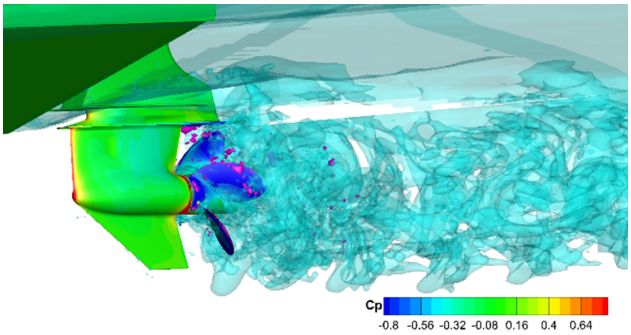

Figure 1: Ventilation and cavitation flows around the propeller of the GPPH using CFDShip-Iowa V5.5 (Park 2022).

Extensive research has been conducted on cavitation flows in previous experimental and computational studies. Most of these studies are primarily focused on steady cavitation flows or unsteady cavitation using a stationary geometry with a fixed angle of attack. Limited research has been carried out on forced unsteady cavitation flows, which are of significant practical importance in marine propulsion systems and control surfaces like propellers, turbines, waterjets, rudders, and hydrofoils (Huang et al 2013; Zhang et al 2020). Unsteady cavitation flows around a pitching foil present a complex phenomenon, which is of more practical relevance to marine propulsion systems as it closely resembles the blade of a propeller operating in a nonuniform wake. Shen and Peterson (1978, 1981) conducted a series of experiments to explore the effects of oscillation on cavitation flows around a pitching foil. In a computational study by Stern (1989), a potential-flow method was employed, and the computed results were compared to the data from these experiments. It was found that the trends of the computed cavity lengths were in accordance with the experiments; however, they were under predicted compared to the observed values. In the study by Huang et al (2013), a NACA66 hydrofoil is used with large angles of attack involving pitching motions with two constant pitching rates. Both experimental and numerical studies are conducted by

Zhang et al (2020) to investigate the cavitating flow structures and hydrodynamics using a Clark-Y hydrofoil. The pitching motion is given by a triangular wave function at a low frequency of 2 Hz.

The objective of the present study is to build upon previous research of the authors for extensions for forced unsteady cavitation and prepare for a numerical investigation of surface piercing propellers, as experimentally studied by Olofsson (1996). The focus will be on conducting numerical simulations of cavitation flows around a pitching foil to develop and validate computational methods for addressing forced unsteady cavitation problems. The geometry used in the present study is the same as employed by the experiments (Shen and Peterson 1978, 1981) mentioned above.

2 COMPUTATIONAL METHODS AND SETUP

2.1 Mathematical Model and Numerical Methods

CFDShip-Iowa V5.5, a fully-coupled multi-phase flow solver, is used for the simulations, which is developed based on the level set single-phase flow solver, CFDShip-Iowa V4.5 (Huang et al 2008). In V5.5, the highly accurate geometric VOF method (Wang et al 2012a,b) is used to replace the LS method for the interface tracking and a fully coupled two-phase flow solver is developed to replace the single-phase solver. A VOF interpolation scheme on the overset grid and a VOF based ghost fluid method are developed to handle the pressure jumps across the interface due to the density changes and surface tension effect (Wang and Stern 2022). The vapor transport mixture cavitation models, e.g., (Zwart et al 2004), have been implemented into V5.5 (Wang et al 2022), where a numerical scheme has been developed for the cavitation models in the framework of a pressure projection method for incompressible Navier-Stokes equations. An algorithm for three-phase, water/vapor/air, interaction is also developed for flows with both ventilation and cavitation, where the VOF method is modified and used to identify the "dry" (air) phase and "wet" (water/vapor mixture) phase, since the cavitation can only occur inside the water phase and the vapor volume fraction is used to distinguish water and vapor phases. Menter's blended $k-\omega/k-\epsilon$ turbulent model (Menter 1994) is adopted for turbulence modeling. A blanking distance (d_{blank}) from the wall is used for the interface functions to handle the moving contact line problem on no-slip boundaries, which is chosen based on the y^+ values (Wang and Stern 2023). The six degrees of freedom (6DOF) equations of motion are solved in the ship-based coordinate system and a dynamic overset grid technique is used to handle grids with relative motions. The overset grid package SUGGAR (Noack 2005) is used for computing the domain connectivity information between overlapping grids.

An implicit second-order Euler backward difference scheme is used for the time derivatives. The convection terms can be discretized using the 1st or 2nd order upwind, 3rd order QUICK, and 4th order upwind schemes, and the 2nd order central difference scheme is used for the diffusion terms. In the present study, the 2nd order scheme is used for the convection terms. The same discretization schemes are used for the turbulence and level set equations. Incompressibility is enforced by a strong pressure/velocity coupling using a Projection (fractional time step) method (Huang et al 2007), and the resulting pressure equation is solved using the Portable Extensible Toolkit for Scientific Computing (PETSc) toolkit. The code is parallelized using the MPI-based domain decomposition approach, where each decomposed block is mapped to one processor. Details of the mathematical models and numerical methods can be found in the above papers and references therein.

2.2 Computational Setup

The geometry of the foil used in the present simulations is the same as the experiments (Shen and Peterson 1978, 1981) as mentioned previously. It is a Joukowski foil of 10.5 percent thickness-to-chord ratio with the chord length of $c = 241mm$. The computations are conducted on a 2D domain of $x/c = [-6.25, 7.75]$ and $z/c = [-1.8971, 1.8971]$ with two blocks of overset grids. The grid size is $353 \times 81 \times 5$ for the body-fitted block and $278 \times 136 \times 5$ for the background block. The sinusoidal pitching motion of the foil is imposed around 25% of the chord from the leading edge. The instantaneous foil angle of attack is given by

$$\alpha = \alpha_0 + \alpha_1 sin\,(\omega t) \tag{1}$$

where α_0, α_1, ω, and t are the mean foil angle, pitch amplitude, circular frequency, and time, respectively. The reduced frequency, k, is defined as

$$k = \omega c/2U \tag{2}$$

Figure 2 shows the geometry of the foil and the overset grid layout. The body-fitted grid oscillates while the background grid remains fixed using a dynamic overset grid technique.

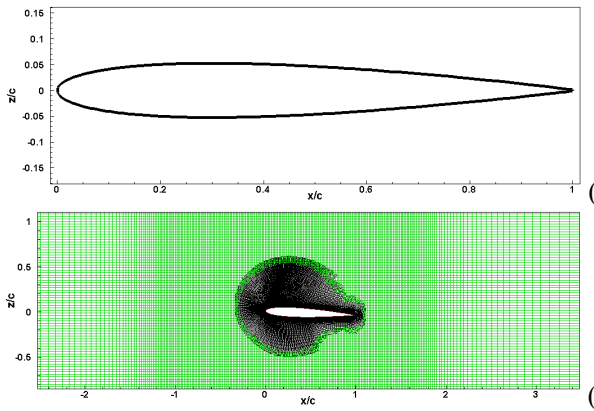

Figure 2: (a) Geometry of the Joukowski foil at the angle of attack of 0^o . (b) Overset grids layout for the pitching foil.

The slip wall boundary conditions are applied at both top and bottom walls, and zero gradient boundary conditions are used for the two sides. Constant pressure and zero velocity gradient are imposed at the inlet of the domain, and constant velocity and zero pressure gradient are specified at the outlet.

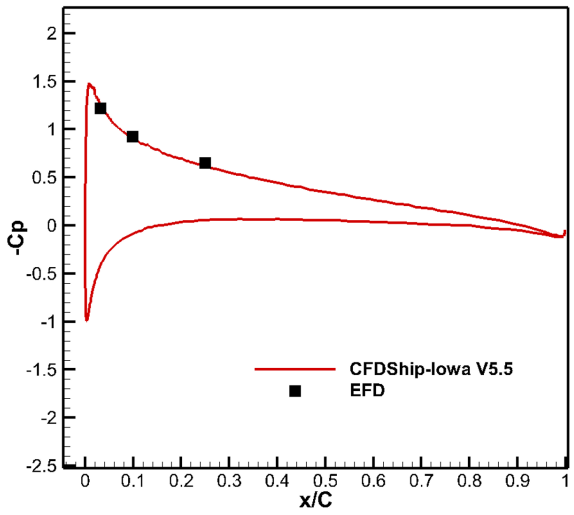

Figure 3: Pressure distribution of the fully wetted foil at a fixed angle of attack of 3.25^o.

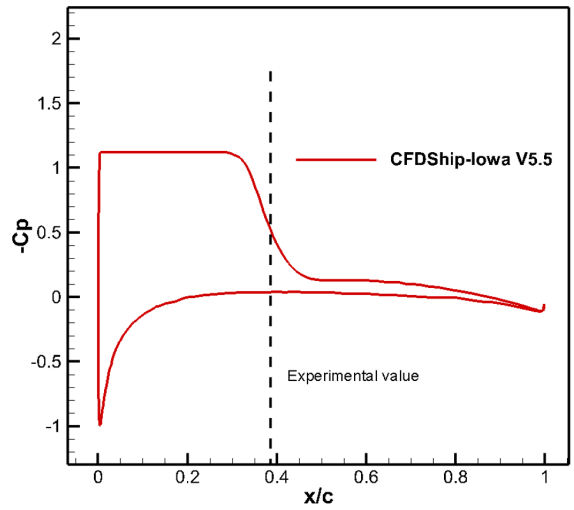

Figure 4: Pressure distribution of the leading cavitation at a fixed angle of attack of 4.25^o.

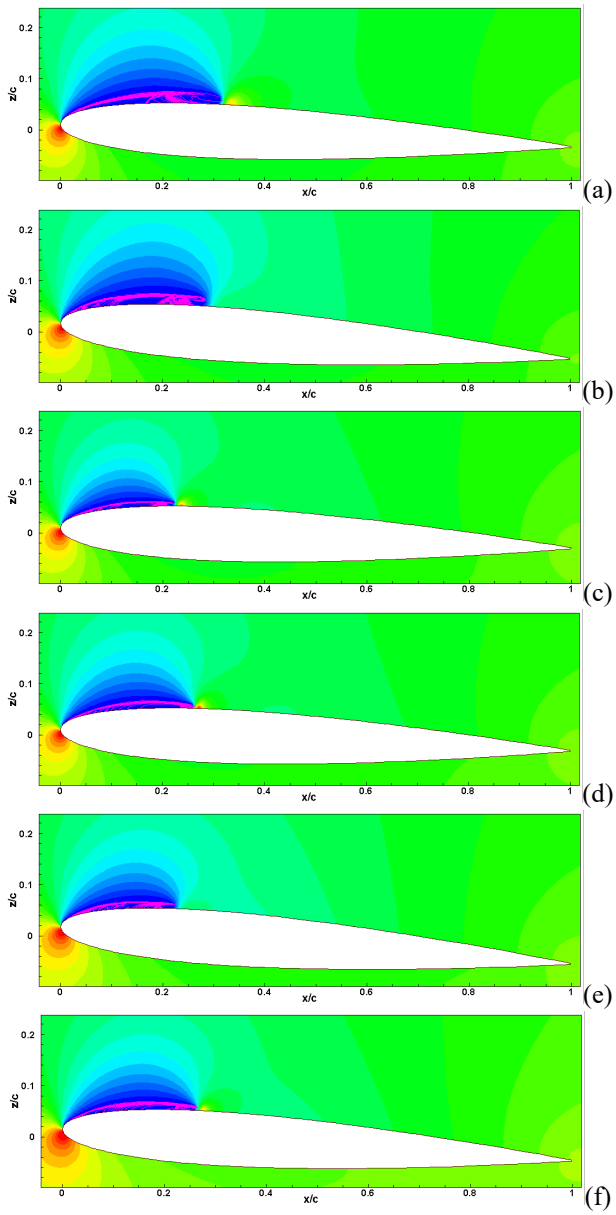

Figure 5: Comparison of the vapor cavity and pressure distribution with different frequencies. From (a) to (f), frequency f = 4, 5.5, 7.5, 10.0, 15.0, and 25.0 Hz.

3 SIMULATION RESULTS AND DISCUSSIONS

3.1 Steady Non-cavitating and Cavitating Simulations

Steady simulations are conducted first for the fully wetted non-cavitating flow at a fixed angle of attack $\alpha = 3.25^o$ and cavitating flow at $\alpha = 4.25^o$. For the fully wetted non-cavitating flow, the Reynolds number is $Re = 1.6 \times 10^6$. For the cavitating flow, the cavitation number is $\sigma = 1.12$ and the Reynolds number is $Re = 2.8 \times 10^6$. The pressure distributions for the non-cavitating and cavitating flows are shown in Figures 3 and 4, respectively. As shown in the figures, the computed pressure distribution for the non-cavitating flow matches the experimental measurement very well. For the cavitating flows, the vapor cavity size based on the pressure distribution also compares well with the experimental observation.

3.2 Unsteady Cavitating Simulations

Imposed oscillations are applied to the foil with the instantaneous angle of attack for the foil given by $\alpha = 3.25^o + 0.95^o sin(\omega t)$. The inlet velocity is $U = 11.49 m/s$ and ambient pressure is $p_\infty = 76.3 kPa$ with the corresponding cavitation number $\sigma = 1.12$ and Reynolds number $Re = 2.8 \times 10^6$, which are the same as used in the steady cavitating simulations. The simulations are carried out with 6 oscillating frequencies $f = 4.0$, 5.5, 7.5, 10.0, 15.0, and 25.0 Hz, which correspond to the reduced frequencies $k =$ 0.264, 0.362, 0.494, 0.659, 0.988, and 1.646. The reduced frequencies chosen cover the range of most practical propeller applications.

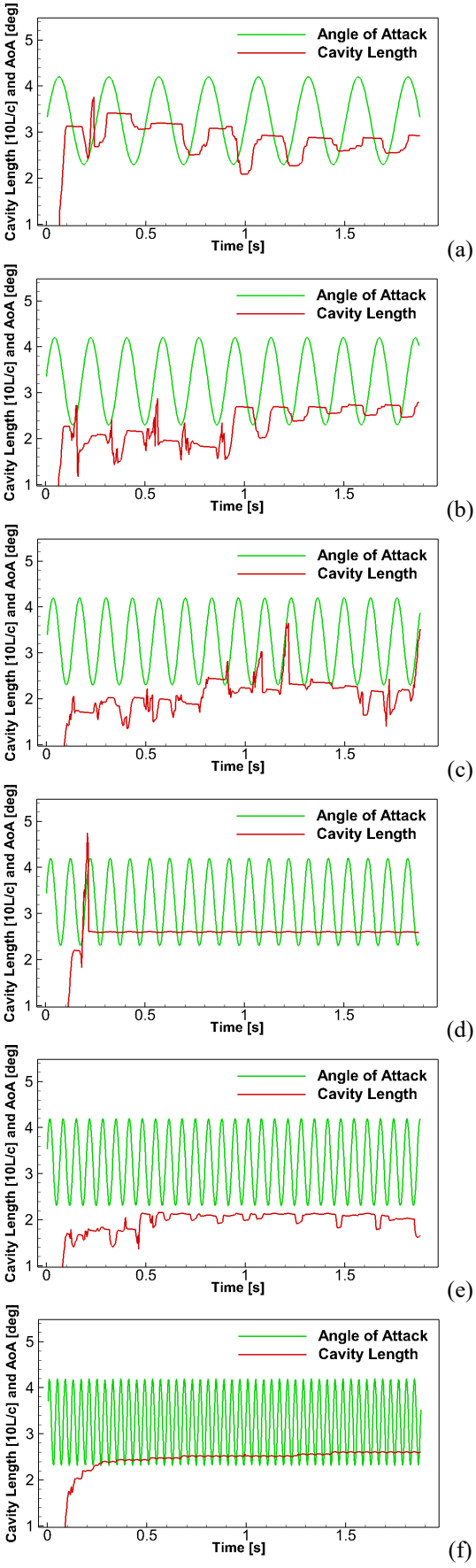

Figure 6: Time history of cavity length and angle of attack for different frequencies. From (a) to (f), frequency $f = 4, 5.5, 7.5, 10.0, 15.0, 25.0Hz$.

Figure 5 shows the water vapor cavities with the maximum length and pressure distributions for various oscillating frequencies, where clear re-entrant jets can be observed for the low and high frequencies. Figure 6 shows the time history of the cavity length along with the angle of attack (α) for different frequencies. Note that the non-dimensional cavity length is magnified by 10 times for illustration purposes. For low oscillating frequencies as shown in the figures, the cavities are very unstable and the cavity size roughly increases after α reaches the maximum value and decreases after the minimum α. For cases with large frequencies, cavities are relatively stable in terms of cavity length.

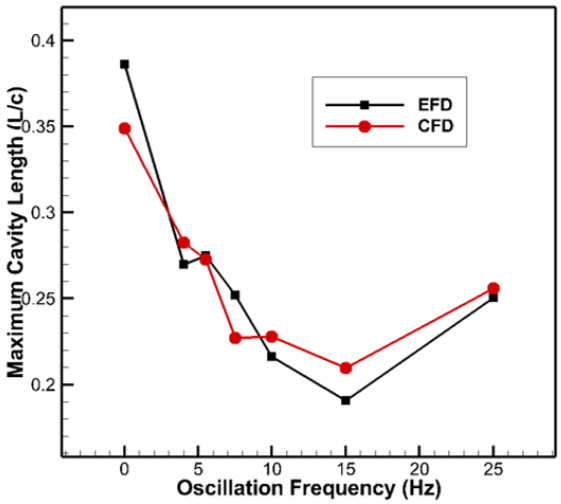

Figure 7: Comparison of the maximum cavity length with the experiment.

The averaged maximum cavity length vs. frequency is shown in Figure 7 including the fixed case with the angle of attack $\alpha = 4.25^o$. As shown in the figure, the computational results generally show the same trend as the experiments, where the cavity length decreases with frequency first and then increases. The computed results show good agreement with the experimental data for most frequencies, except for the case at f = 7.5 Hz, where the cavitation exhibits significant instability as shown in Figure 6(c). It's important to note that the experimental data is obtained based on visual observations. In the unstable region, the simulations are highly sensitive to the numerical treatment, such as boundary conditions and wave blanking distance used for handling the moving contact line problem (Wang and Stern 2023). In the present study, the wave blank value is chosen to satisfy $y^+ = 24$.

Figure 8 shows the time history of lift force along with angle of attack for different oscillating frequencies. As shown in the figures, the lift forces exhibit the same frequency and phase of oscillations as the angle of attack. At low frequencies, the lift force also shows instability especially at $f = 7.5Hz$, which is also demonstrated for the cavity length in Figure 6. Again, the lift forces show relatively stable solution for high frequencies. These instabilities at low frequencies are probably related to the interactions between the foil oscillation and cavity natural frequency. If

the frequency of foil oscillation is close to the natural frequency of the cavity, the flow tends to be unstable and the cavity also has sufficient time to respond to the foil oscillation at low frequencies (Stern 1989).

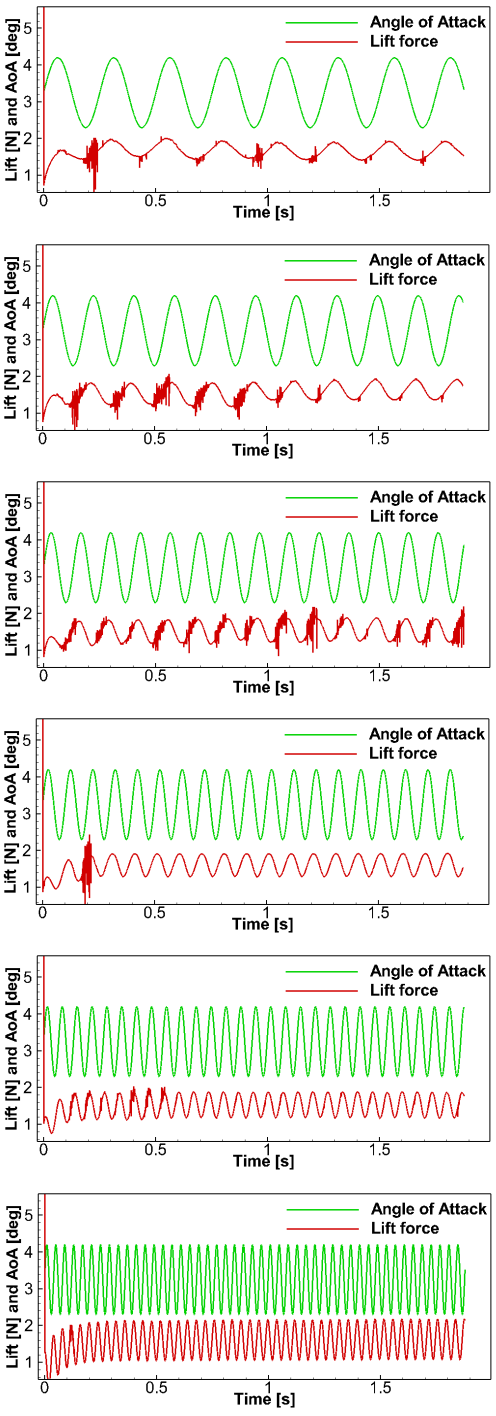

Figure 8: Time history of lift force and angle of attack for different frequencies. From (a) to (f), frequency $f = 4, 5.5, 7.5, 10.0, 15.0, 25.0Hz$**.**

Comparison of the lift forces at different frequencies is shown in Figure 9. The amplitude, maximum, and mean of the lift force are shown in Figure 10. As shown in the figures, the oscillation amplitude of the lift generally increases with the frequency. Both the maximum and mean values of the lift roughly decrease with frequency first and then increase except at $f = 7.5Hz$. Note that the numerical results of both the maximum cavity length and lift force show a drop at frequency $f = 7.5Hz$. This might be an indication that the natural frequencies of the cavity differ between experimental and numerical results. Further investigation is needed for the future work. The mean lift shows a similar trend as the maximum cavity length, i.e., both have the maximum value at the lowest frequency $f = 4.0Hz$ and minimum value at $f = 15.0Hz$. This is understandable since the lift force increases with the cavity size.

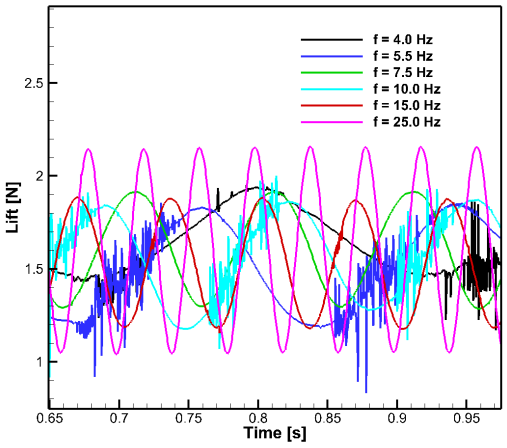

Figure 9: Comparison of the lift forces for different frequencies.

It should be noted that numerical simulations of such high-speed cavitation flows are challenging and difficult since multi-phase flows occur in the turbulent boundary layer and interact with the oscillating bodies with complex geometry. Although the CFD maximum cavity length agrees well with the EFD data (based on visual observations), the results are very sensitive to the numerical treatments, such as boundary conditions, wave blanking distance, turbulence model wall treatment, cavitation empirical coefficients, grid resolutions, density and viscosity estimation, etc., which also affect the stability and convergence of the simulations. Constant velocity and pressure boundary conditions are usually used at the inlet or outlet, however, for unsteady oscillating flows, the velocity and pressure also oscillate at the inlet and outlet. Wave blanking distance is used in CFDShip-Iowa for the contact line problem and to force $k-\omega$ model near the wall for SST turbulence model, which significantly affects the convergence of the code and cavity length. The cloud cavitation is not captured in the present simulations due to the RANS turbulence and mixture cavitation models used. The accuracy of homogeneous mixture cavitation models relies on the empirical coefficients which need to be tuned for different flow conditions. Further investigation is needed with a focus on refining the numerical treatments, improved scale resolved turbulence models for multi-phase flows, and high-fidelity cavitation model using a sharp interface method for better resolved unsteady cavitation flows.

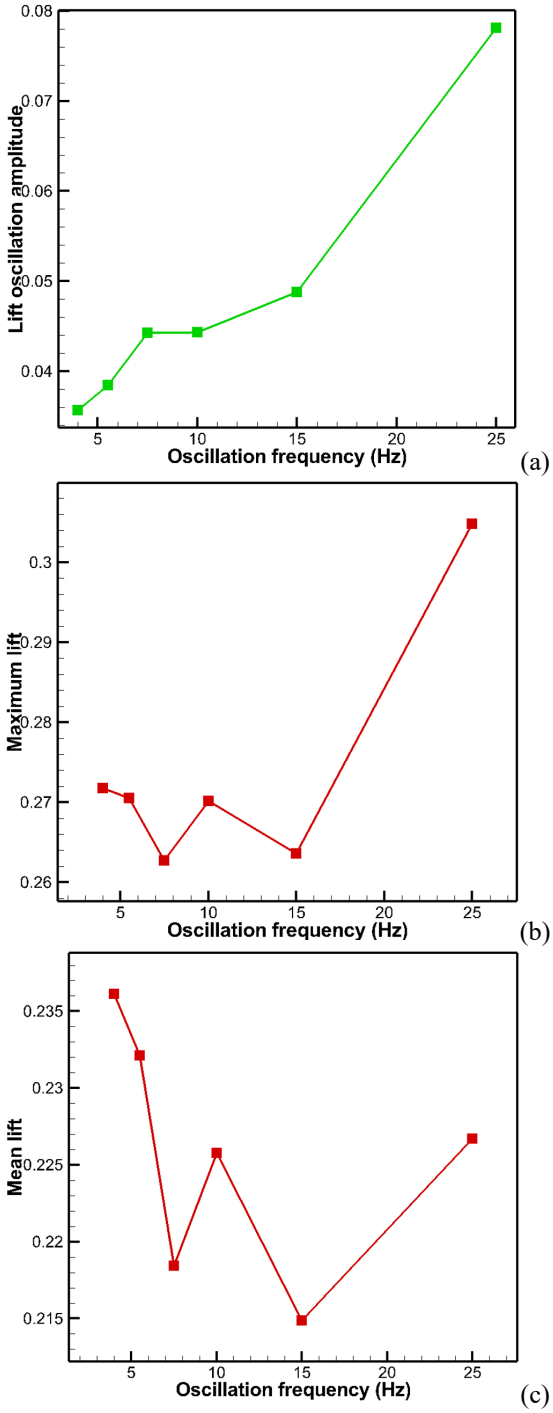

Figure 10: (a) Amplitude of the lift force. (b) Maximum lift force. (c) Mean lift force.

4 SUMMARY AND DISCUSSIONS

In this study, numerical simulations of the unsteady cavitation flows around a 2D pitching foil are performed using CFDShip-Iowa V5.5. Sinusoidal pitching motions are imposed to the foil with reduced frequencies, $k = 0.264$, 0.362,0.494,0.659,0.988, and 1.646, and pitch amplitude $\alpha_1 = 0.95^o$ in the same range of most practical propeller applications. The effect of the pitching frequency on the cavity size and lift force is investigated.

It has been found that the maximum cavity length decreases with the reduced frequency first and then increases, which is in good agreement with the experimental observations. The simulation results show that the cavity is very unstable at low oscillating frequencies and tends to be stable at high frequencies. These instabilities at low frequencies are probably related to the interactions between the foil oscillation and cavity natural frequency. If the frequency of foil oscillation is close to the natural frequency of the cavity, the flow tends to be unstable and the cavity also has sufficient time to respond to the foil oscillation at low frequencies.

The lift force exhibits the same oscillating frequency and phase as the angle of attack. The amplitude of the lift increases with the frequency, the maximum and mean values of the lift decrease with the frequency first and then increase. The mean lift shows similar a trend as the maximum cavity length.

Numerical simulations of such forced unsteady cavitation flows are challenging and difficult. The results are very sensitive to the numerical treatments, which also affect the stability and convergence of the simulations. Further investigation is needed with a focus on refining the numerical treatments and examining the physics of forced unsteady cavitation in conjunction with the available experimental data. In the future work, improved and scale resolved turbulence models for multi-phase flows will be considered for better resolved unsteady cavitation turbulent flows. The high-fidelity cavitation model using a sharp interface method (e.g., VOF) will be considered. Extension to the numerical investigation of surface piercing propellers will be made including forced unsteady cavitation and ventilation.

ACKNOWLEDGEMENTS

This work is supported by the Office of Naval Research grants N00014-20-1-2259 and N00014-22-1-2413 under the administration of Dr. Robert Brizzolara. The simulations were performed using DoD DSRC HPCMP resources, including FY23 Pathfinder program allocations.

REFERENCES

Brizzolara, S., Wang, Z., Stern, F. & Cura Hochbaum, A. (2022). 'Multiphase CFD of super-cavitating surface-piercing hydrofoils'. Proceedings of the 34th Symposium on Naval Hydrodynamics , Washington D.C., USA.

Huang, B., Ducoin, A. & Young, Y. L. (2013). 'Physical and numerical investigation of cavitating flows around a pitching hydrofoil'. Physics of Fluids **25**(10).

Huang, J., Carrica, P. M. & Stern, F. (2007). 'Coupled ghost fluid/two-phase level set method for curvilinear body-fitted grids'. International Journal for Numerical Methods in Fluids **55**(9), pp. 867–897.

Huang, J., Carrica, P. M. & Stern, F. (2008). 'Semi-coupled air/water immersed boundary approach for curvilinear dynamic overset grids with application to ship hydrodynamics'. International Journal for Numerical Methods in Fluids **58**(6), pp. 591–624.

Menter, F. R. (1994). 'Two-equation eddy-viscosity turbulence models for engineering applications'. AIAA Journal **32**, pp. 1598–1605.

Noack, R. (2005). 'SUGGAR: A general capability for moving body overset grid assembly'. Proceedings of the 17th AIAA computational fluid dynamics conference , Toronto, Canada.

Olofsson, N. (1996). Force and flow characteristics of a partially submerged propeller. PhD thesis, Chalmers University of technology, Gotborg, Sweden.

Park, S. (2022). Free Running 6 Degree of Freedom CFD for High-Speed Small Craft. PhD thesis, The University of Iowa, Iowa City, IA, USA.

Shen, Y. T. & Peterson, F. B. (1978). 'Unsteady cavitation on an oscillating hydrofoil'. Proceedings of the 12th ONR Sym. Naval Hydrodynamics , Washington DC, USA.

Shen, Y. T. & Peterson, F. B. (1981). 'The influence of hydrofoil oscillation on boundary layer transition and cavitation noise'. Proceedings of the 13th ONR Sym. Naval Hydrodynamics , Tokyo, Japan.

Stern, F. (1989). 'Comparison of Computational and Experimental Unsteady Cavitation on a Pitching Foil'. Journal of Fluids Engineering **111**(3), pp. 290–299.

Stern, F., Diez, M., Wang, Z., Lee, E. J. & Kubina, E. R. (2022). 'Digital design: The way forward'. Proceedings of the AVT-366 Research Workshop , Sibiu, Romania.

Wang, Z., Park, S. & Stern, F. (2022). 'Cavitation implementation algorithms based on pressure projection method for incompressible flows with three-phase interactions'. Proceedings of the 7th International Symposium on marine Propulsors , Wuxi, China.

Wang, Z. & Stern, F. (2022). 'Volume-of-fluid based two-phase flow methods on structured multiblock and overset grids'. International Journal for Numerical Methods in Fluids **94**(6), pp. 557–582.

Wang, Z. & Stern, F. (2023). 'Moving contact line and no-slip boundary conditions for high-speed planing hulls'. Proceedings of the X International Conference on Computational Methods in Marine Engineering, MARINE 2023 , Madrid, Spain.

Wang, Z., Yang, J. & Stern, F. (2012a). 'A new volume-of-fluid method with a constructed distance function on general structured grids'. J. Comp. Phys. **231**, pp. 3703–3722.

Wang, Z., Yang, J. & Stern, F. (2012b). 'A simple and conservative operator-splitting semi-lagrangian volume-of-fluid advection scheme'. J. Comp. Phys. **231**, pp. 4981–4992.

Zhang, M., Biao, H., Zhongdong, Q., Taotao, L., Qin, W., Hanzhe, Z. & Guoyu, W. (2020). 'Cavitating flow structures and corresponding hydrodynamics of a transient pitching hydrofoil in different cavitation regimes'. International Journal of Multiphase Flow **132**, pp. 103408.

Zwart, P. J., Gerber, A. G. & Belamri, T. (2004). 'A two phase flow model for predicting cavitation dynamics'. Proceedings of the Fifth international conference on multiphase flow , Yokohama, Japan.